

Quadrupolar spectra of nuclear spins in strained InGaAs quantum dots

Ceyhun Bulutay^{1,2,*}

¹*Department of Physics, Bilkent University, Ankara 06800, Turkey*

²*Institute of Quantum Electronics, ETH-Zürich, CH-8093 Zürich, Switzerland*

(Dated: January 12, 2019)

Self-assembled quantum dots (QDs) are born out of lattice mismatched ingredients where strain plays an indispensable role. Through the electric quadrupolar coupling strain affects the nuclear spins. To guide prospective single-QD nuclear magnetic resonance (NMR) as well as dynamic nuclear spin polarization experiments, an atomistic insight to the strain and quadrupolar field distributions is presented. A number of implications of the structural and compositional profile of the QD have been identified. A high aspect ratio of the QD geometry enhances the quadrupolar interaction. The inclined interfaces introduce biaxiality and the tilting of the major quadrupolar principal axis away from the growth axis; the alloy mixing of gallium into the QD enhances both of these features while reducing the quadrupolar energy. Regarding the NMR spectra, both Faraday and Voigt geometries are investigated, unraveling in the first place the extend of inhomogeneous broadening and the appearance of the normally-forbidden transitions. Moreover, it is shown that from the main extend of the NMR spectra the alloy mole fraction of a single QD can be inferred. By means of the element-resolved NMR intensities it is found that In nuclei has a factor of five dominance over those of As. In the presence of an external magnetic field, the borderlines between the quadrupolar and Zeeman regimes are extracted as 1.5 T for In and 1.1 T for As nuclei. At these values the nuclear spin depolarization rates of the respective nuclei get maximized due to the noncollinear static hyperfine interaction with a resident electron in the QD.

PACS numbers: 75.75.-c, 76.60.Gv, 76.60.Pc

I. INTRODUCTION

In the coherent control of electron spins within a solid state environment, such as in quantum dots (QDs), the nuclear spin reservoir acts as the main source of decoherence.¹⁻³ Recent studies now assure that nuclear spin bath can be tamed so as to counter the detrimental effect it may have on the carrier spins.⁴⁻⁸ Therefore, in the emerging state of understanding, an alternative is to utilize nuclear spins as a resource, for instance as a natural qubit memory (for an extended review and references, see, Ref. 9). In these studies, self-assembled QDs have been one of the archetypal systems. Within the full gamut of possible combinations of self-organized materials,¹⁰ the InAs on GaAs system stands out due to extensive research efforts devoted over more than a decade to their growth and optoelectronic characterizations.¹¹ For the purposes of controlling the spin dynamics in InAs QDs, several groups¹²⁻²⁴ have studied various aspects of the optical orientation²⁵ of an electron spin and its transfer to the nuclear spins via the hyperfine interaction leading to the dynamic nuclear spin polarization.²⁶

One of the remarkable achievements that paved the way to the coherent manipulation of nuclear spin dynamics has been the nuclear magnetic resonance (NMR) of a *single* QD.^{27,28} With further improved precision, position selective control of small groups of nuclear spins inside a dot is being pursued.²⁹ This so-called optically detected NMR is initiated by the circularly polarized excitation of a spin-polarized electron spin inside a QD that polarizes the nuclear spins through the hyperfine interac-

tion. The Overhauser field established by the polarized nuclei acts back on the electronic system which can be externally measured over an excitonic Zeeman splitting. Additionally if an rf magnetic field resonant with nuclear spin transitions is incident, it depolarizes some of the nuclear spins reducing the Overhauser field, which can in turn be detected from a shift in the optical emission spectra. Along this line, a recent demonstration utilized a sequence of two phase-locked rf pulses to induce coherent rotations of a targeted group of nuclear spins optically pumped to a high polarization degree.³⁰ The advantage of this technique is that it enables full coherent control over the Bloch sphere and yet on the order of microsecond time scales.

These NMR experiments were performed on GaAs interface-fluctuation QDs with the deliberate aim of avoiding any strain to keep the resonances narrow.^{29,30} On the other hand strain is an integral part of self-assembled InAs QDs.¹¹ The existing negative sentiments for the strain in the context of electron and nuclear spin dynamics have been dramatically reversed by the work of Dzhioev and Korenev.³¹ As a matter of fact, several decades ago it was experimentally shown that anisotropic strain in a III-V crystal lattice causes local electric field gradients (EFG) with which a spin- I nucleus with $I \geq 2$ interacts because of its quadrupolar moment.³²⁻³⁴ This quadrupolar interaction (QI) splits the nuclear spin degeneracy even in the absence of an external magnetic field,^{35,36} hence it energetically suppresses the nuclear spin flip events, stabilizing the electron spin orientation confined in the QD.³¹ With the new vision this has brought, strain need not be a nuisance but can be harnessed as a new degree of freedom giving richness to InAs

QDs.

The aim of this work is to offer an atomistic understanding of the interesting physics arising from the co-existence of QI together with the dc and rf magnetic fields. This is in accord with the current progress of the experimental techniques having the goal to address and control relatively few number of nuclei within a QD.^{29,30} Starting from the behavior of the spatial variation of the strain tensor, we trace the factors that affect QI, and identify primarily the high aspect ratio of the QD as a factor for enhancing it. Considering different magnetic field orientations and the effect of random alloy mixing i.e., $\text{In}_x\text{Ga}_{1-x}\text{As}$ QDs, critical insight is gained on the vulnerability of each nuclear spin transition in the NMR spectrum under inhomogeneous broadening. As one of the hitherto standing issues, the mole fraction of the constituents can vary appreciably from dot to dot within the same sample,^{37,38} rendering the in situ compositional identification of a targeted QD so far not practical. We demonstrate that this can be readily extracted from the main span of the NMR spectra. Moreover, our element-resolved spectra present crucial information for the labeling of the features in the rather complicated overall spectra. For the typical QD parameters reported in relevant experiments, we extract an effective quadrupolar field, B_Q of 1.5 T (1.1 T) for the In (As) nuclei, as a borderline below which QI dominates. The atomistic picture that we acquire also provides us the distribution of the quadrupolar principal axes within the QD. We make use of this information in working out the nuclear spin depolarization due to noncollinear static hyperfine interaction arising from the tilting of the major quadrupolar axis from the optical axis. The depolarization time drops to a minimum on the order of an hour at the magnetic field coinciding with B_Q , as a manifestation of the strong competition between the QI and the Zeeman field at this value.

The paper is organized as follows. In Sec. II we give the theoretical details for the strain, QI, and the nuclear spin depolarization. In Sec. III some information about our QD structures is given, followed by the results grouped into strain and quadrupolar splittings, NMR spectra, and the noncollinear static hyperfine interaction. In Sec. IV we summarize our conclusions, and append a section on the matrix elements for obtaining the energy spectra and the rf-initiated nuclear spin transitions under an arbitrary EFG.

II. THEORY

A. Strain

From a computational point of view, to identify the strain profile, the ionic relaxation of the QD and the host matrix atoms is needed. This is accomplished by molecular statics as implemented in the LAMMPS code.³⁹ Here, the main input is the semi-classical force field that gov-

erns the atomic interactions. The preferred choice for group IV and III-V semiconductors are the Abell-Tersoff potentials.⁴⁰ We make use of the recent parametrization by Powell *et al.* who fitted their force field expression to a large set of cohesive and elastic properties calculated from density functional theory.⁴¹ With these tools and for a chosen compositional profile, the equilibrium atomic positions become readily available.⁴² Next, one needs to extract the strain state, again in an atomistic level as we aim for the EFGs at each nuclear site. Among the several possible strain measures, we adopt the one proposed by Pryor *et al.* because of its inherent compatibility with tetrahedral bonds, as in the present case.⁴³ In this measure, the critical task is to correctly align an unstrained reference tetrahedron for each local bonding topology. This local strain attains a very rapid variation especially for the random alloy mixing of $\text{In}_x\text{Ga}_{1-x}\text{As}$. Therefore, like Bester *et al.*,⁴⁴ we average the strain tensor; in our case over the twelve neighboring same-ionicity sites which we also apply to the pure InAs QDs as well.

B. Quadrupolar interaction

In the linear elastic limit, we can express the EFG tensor components V_{ij} in any orthogonal coordinate frame⁴⁵ using the computed local strain tensor ϵ_{ij} as:

$$V_{ij} \equiv \frac{\partial^2 V}{\partial x_i \partial x_j} = \sum_{k,l=1}^3 S_{ijkl} \epsilon_{kl}, \quad (1)$$

where S is the fourth-rank gradient elastic tensor.^{46,47} Transforming this tensor expression to Voigt notation in the cubic crystallographic frame we get

$$V_\mu = \sum_{\nu=1}^6 S_{\mu\nu} \epsilon_\nu. \quad (2)$$

As the trace of the EFG is unobservable⁴⁹ it is conveniently set to zero, $\sum_i V_{ii} \rightarrow 0$ which leads to $S_{11} = -2S_{12}$. This results in the following explicit relations for the EFG tensor components in the mixed Voigt and tensor notation

$$V_{zz} = S_{11} \left[\epsilon_{zz} - \frac{1}{2} (\epsilon_{xx} + \epsilon_{yy}) \right], \quad (3)$$

$$V_{xy} = V_{yx} = 2S_{44} \epsilon_{xy}, \quad (4)$$

with the remaining components being obtained by their cyclic permutations.⁵⁰ The EFG tensor couples to the nuclear quadrupole moment tensor (operator) $\mathcal{Q}_{\alpha\beta}$ through the Hamiltonian³⁶

$$\begin{aligned} \mathcal{H}_Q &= \frac{1}{6} \sum_{\alpha,\beta} V_{\alpha\beta} \mathcal{Q}_{\alpha\beta}, \\ &= \frac{eQ}{6I(2I-1)} \sum_{\alpha,\beta} V_{\alpha\beta} \left[\frac{3}{2} (\mathcal{I}_\alpha \mathcal{I}_\beta + \mathcal{I}_\beta \mathcal{I}_\alpha) - \delta_{\alpha\beta} \mathcal{I}^2 \right], \end{aligned}$$

where \mathcal{I} is the dimensionless spin operator, e is the electronic charge, and Q is the electric quadrupole moment of the nucleus. This expression gets simplified in the EFG principal axes frame ($V_{IJ} \equiv 0$, for $I \neq J$) as

$$\mathcal{H}_Q = \frac{e^2 q Q}{4I(2I-1)} \left[3\mathcal{I}_Z^2 - \mathcal{I}^2 + \eta \frac{\mathcal{I}_+^2 - \mathcal{I}_-^2}{2} \right], \quad (5)$$

where $\mathcal{I}_\pm \equiv \mathcal{I}_X \pm i\mathcal{I}_Y$, $q \equiv V_{ZZ}/e$ is the field gradient parameter, and $\eta = (V_{XX} - V_{YY})/V_{ZZ}$ is the biaxiality (asymmetry) parameter. The former is the primary coupling constant of QI, and the latter determines the mixing between the free nuclear spin magnetic quantum numbers. In the most general case that we shall consider, in addition to quadrupolar part \mathcal{H}_Q , a nuclear spin will have interactions with dc and rf magnetic fields in the form $\mathcal{H}_M = -\gamma\hbar\mathcal{I} \cdot \mathbf{B}_0$ and $\mathcal{H}_{\text{rf}} = -\gamma\hbar\mathcal{I} \cdot \mathbf{B}^{\text{rf}} \cos\omega_{\text{rf}}t$, where γ is the gyromagnetic ratio of the nucleus. The weak rf part can safely be treated perturbatively, whereas the dc magnetic field can be strong and gives rise to Zeeman effect; we shall abbreviate the stationary states under both quadrupolar and Zeeman splittings as the QZ spectra.⁵² Individual matrix elements for obtaining the QZ spectra for an arbitrary EFG and \mathbf{B}_0 as well as the \mathcal{H}_{rf} -initiated transition rates are given in the Appendix section.

C. Noncollinear static hyperfine interaction

Quite commonly in the nuclear spin experiments there exists an electron in the QD with an optically oriented spin along the growth axis.^{12–24} Through the hyperfine interaction it then polarizes the QD nuclear spins, termed as the dynamic nuclear polarization.²⁶ Deng and Hu have suggested that in the presence of quadrupolar mixing a new spin depolarization channel becomes possible through the hyperfine coupling.⁵³ If we leave out the weaker anisotropic dipolar part in the s -type conduction band of III-V semiconductors,⁵⁴ the hyperfine interaction can be represented by the isotropic Fermi contact term⁵⁵

$$\mathcal{H}_{\text{hf}} = \sqrt{f_e} A_{\text{hf}} |\psi(\mathbf{R})|^2 \left[\underbrace{\mathcal{I}_z \mathcal{S}_z}_{\text{static}} + \frac{1}{2} \underbrace{(\mathcal{I}_+ \mathcal{S}_- + \mathcal{I}_- \mathcal{S}_+)}_{\text{dynamic}} \right], \quad (6)$$

where $\mathcal{S}_z, \mathcal{S}_\pm$ are the z -component and the raising/lowering electron spin operators, A_{hf} is the hyperfine constant of the nucleus, f_e is the average fraction of the time electron is inside the QD (i.e., hyperfine interaction is on) for which we use the value 0.035.^{55,56} At a nuclear site, \mathbf{R} , $\psi(\mathbf{R})$ is the electron wave function, that we simply approximate with a height-dependent Gaussian profile over the QD as $\psi(\rho, z) \propto e^{-(3\rho/D(z))^2}$, where $D(z)$ is the z -dependent diameter of the truncated cone-shaped QD.

The dynamic part of \mathcal{H}_{hf} which is responsible for the spin flip-flops as a direct process becomes energetically

impossible due to the presence of the external magnetic field and the large energy mismatch between nuclear and electronic Zeeman energies. On the other hand in the noncollinear case of major EFG principal axis being tilted from the growth axis the static part becomes much more interesting. When we express \mathcal{I}_z operator in EFG-coordinate components we observe that this allows a nuclear spin transition *without* changing the spin orientation of the electron. There is still an energy cost for the nuclear spin flip but this is much less compared to dynamic term being on the order of a few neV which is negligible compared to the spontaneous lifetime broadening of $\Delta_l \sim 1 \mu\text{eV}$ of the exciton state in the optically created electron spin pumping configuration.⁵⁷ Therefore, the rate of noncollinear static hyperfine interaction (NC-SHFI) can become significant. For a transition from state $|i\rangle$ to $|j\rangle$, this rate is given by

$$W_{ji}^{\text{NCSHF}} = f_e [A_{\text{hf}} |\psi(\mathbf{R})|^2]^2 |\langle j | \mathcal{I}_z | i \rangle|^2 \times \frac{2\Delta_l/\hbar}{(E_j - E_i)^2 + \Delta_l^2}. \quad (7)$$

III. RESULTS

A. Test structures

There exists a plethora of different realizations for the compositional and structural profiles of the self-assembled QDs; for a very recent experimental review, see, Ref. 37, and specifically for the InAs QDs we refer to Ref. 38. Guided by the samples used in recent nuclear spin experiments,^{12–24} we center our discussion around a QD of a truncated cone shape⁵⁸ with a base (top) diameter 25 nm (10 nm), placed over a 0.5 nm wetting layer, all fully embedded in a GaAs host lattice. The computational supercell contains some 1,800,000 atoms, most of which for the host matrix region, with the InAs QD region having 16,702 In and 15,432 As atoms. In the case of alloy mixing discussions, we randomly replace a fraction of the In atoms with Ga atoms. We start from a uniform compressive strain in the QD region by setting its lattice constant to that of bulk GaAs. During the energy minimization we use periodic boundary conditions while allowing for the computation box to shrink and expand, so as to attain a zero pressure on the walls.⁵⁹ After this relaxation the InAs QD height settles to 2.93 nm. Our choice for such a high-aspect-ratio QD is again guided by the samples used in relevant experiments.^{12–24} In order to extract the dependence on the aspect ratio and alloy composition of the QDs, different heights and indium mole fractions are considered as well.

B. Strain and quadrupolar splitting

To have a broad overview, we would like to start with Fig. 1 displaying the atomistic profiles over (100) and

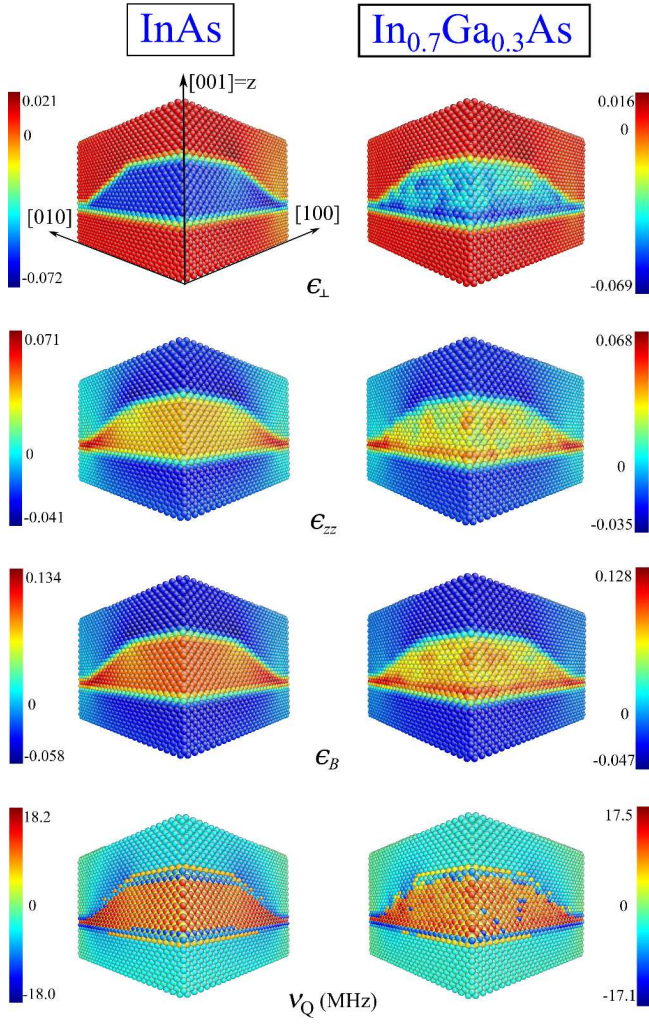


FIG. 1. (Color online) Atomistic profiles⁶⁰ over (100) and (010) cross sections for InAs and $\text{In}_{0.7}\text{Ga}_{0.3}\text{As}$ QDs. Bigger spheres correspond to In atoms.

(010) cross sections of InAs and $\text{In}_{0.7}\text{Ga}_{0.3}\text{As}$ QDs. A compressive in-plane strain, ϵ_{\perp} is seen to be mainly preserved after relaxation whereas for ϵ_{zz} it is released along the growth axis to its environs leaving the QD region with a tensile ϵ_{zz} value. The opposite signs for the in-plane and growth axis QD strain components is a reflection of the Poisson effect.⁶¹ Thus, with the biaxial strain defined as $\epsilon_B \equiv \epsilon_{zz} - (\epsilon_{xx} + \epsilon_{yy})/2 = \epsilon_{zz} - \epsilon_{\perp}$, a compressive value follows directly from these two. It can be observed by comparing left and right panels in Fig. 1 that the compositional variation does not lead to a qualitative change on the strain behavior. In the case of quadrupolar energy parameter, ν_Q the variation among different elements is substantial, while those within each element simply follows that of the biaxial strain.

To support these observations with more quantitative data, in Table I the strain and quadrupolar statistics of the InAs QD atoms are summarized. Considering that a carrier within the QD will mainly sample the core

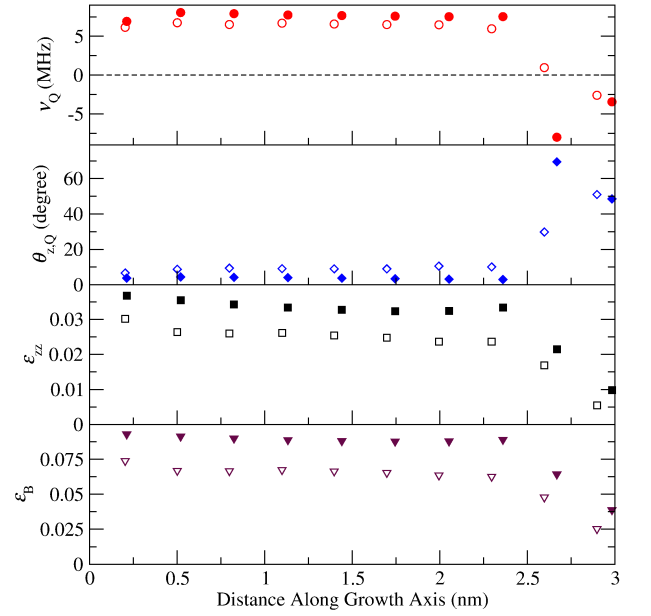


FIG. 2. (Color online) Monolayer-averaged axial variations of ϵ_B , ϵ_{zz} , $\theta_{z,Q}$, and ν_Q along the growth axis starting from the base of the QD without including the wetting layer. Filled (hollow) symbols are for InAs ($\text{In}_{0.7}\text{Ga}_{0.3}\text{As}$) QD. The Gaussian envelope square weighting is used for the contribution of atomistic quantities within each monolayer.

of the confinement region, we provide an electron wave function-square-weighted statistics, assuming a Gaussian profile with the aforementioned quantitative form. Contrasting In and As atoms, most strain components look very similar. The exception to this is the shear strain measure that we define as $\epsilon_S \equiv |\epsilon_{xy}| + |\epsilon_{yz}| + |\epsilon_{zx}|$ which is significantly larger for As. This is caused by those As atoms on the interface forming *heterobonds* with In and Ga atoms. The shear strain is known to be crucial for the piezoelectric field,⁶² whereas in this context it also causes the tilting of the quadrupolar axes. Regarding the angular behavior, first of all the strain major principal axis lies almost on the in-plane direction which is due to the dominance of ϵ_{\perp} . As a direct consequence of this strain profile, and in particular due to the relation $V_{zz} = S_{11}\epsilon_B$, the EFG major principal axis is oriented very close to the growth direction. In contrast, for the V_{xx} and V_{yy} EFG components, the strain components ϵ_{xx} and ϵ_{yy} appear in opposite signs and largely cancel. A curious discrepancy between In and As occurs for the tilting angle of the major quadrupolar axis from the growth direction, $\theta_{z,Q}$: This angle is about eight times larger for As than In. The tilting is caused by the shear EFG components, and the discrepancy between In and As mainly follows from the S_{44} coefficients which are 10.0×10^{15} statcoulomb/cm³ and 25.855×10^{15} statcoulomb/cm³, respectively.³⁴ In addition, as mentioned before, shear strain is also larger for As, and hence, the larger deviation of the As major quadrupolar axis from the growth axis. As an indirect consequence of this, As system has twice as large

TABLE I. The mean and standard deviation for certain atomistic quantities of the considered InAs QD. ϵ_{\perp} : in-plane strain perpendicular to growth axis, ϵ_S : shear strain, ϵ_B : biaxial strain, ν_Q : quadrupolar (lowest) energy splitting, η : EFG biaxiality parameter, $\theta_{z,\epsilon}$: polar angle the strain major principal axis makes with the growth axis, $\theta_{z,Q}$: polar angle the quadrupolar major principal axis makes with the growth axis. Envelope-square-weighted statistics are given, while the raw (equal-weighted) values are quoted in parentheses.

	Indium		Arsenic	
	Mean	Standard Deviation	Mean	Standard Deviation
ϵ_{\perp}	-0.057 (-0.054)	0.005 (0.012)	-0.056 (-0.055)	0.004 (0.007)
ϵ_S	0.004 (0.008)	0.004 (0.005)	0.005 (0.010)	0.004 (0.006)
ϵ_B	0.090 (0.088)	0.010 (0.018)	0.086 (0.084)	0.013 (0.020)
ν_Q (MHz)	3.974 (4.074)	0.427 (0.801)	9.804 (8.256)	6.322 (8.955)
η	0.042 (0.080)	0.041 (0.085)	0.117 (0.255)	0.198 (0.272)
$\theta_{z,\epsilon}$	89.3° (86.8°)	2.3° (8.0°)	88.0° (87.6°)	1.6° (3.4°)
$\theta_{z,Q}$	1.7° (2.7°)	1.6° (2.8°)	12.9° (23.7°)	24.1° (30.6°)

EFG biaxiality, $\eta = (V_{XX} - V_{YY})/V_{ZZ}$ compared to In (cf. Table I). Another marked difference is about the quadrupolar energy gaps. If we temporarily assume a uniaxial case ($\eta \rightarrow 0$), the energy difference between $m = \pm 1/2$ and $m = \pm 3/2$ levels becomes $h\nu_Q = 3e^2qQ/[2I(2I - 1)]$. This energy is more than thrice as large for As (~ 8.3 MHz) compared to In (~ 4 MHz). The underlying reason is that In has $I = 9/2$ whereas As has $3/2$ nuclear spins. The Q values are however in favor of In, which has 0.860×10^{-24} cm² compared to As having 0.27×10^{-24} cm².³⁴ As a matter of fact, if one considers the *full* nuclear spin manifold energy span under QI, i.e., between $m = \pm 1/2$ and $m = \pm I$, In has an extend of ~ 36 MHz which is about four times larger than that of As. If we now focus on the difference between envelope-square- and equal-weighted (in parantheses) results, the main deviations are seen to be on the shear strain, EFG tilt angles and biaxiality values which indicate that there comes a substantial contribution from the inclined interface regions in the case of equal-weighted statistics. Also note that standard deviation for all quantities are higher when the interface region is included (i.e., under equal-weighted statistics).

Next, in Fig. 2 we return to the effect of alloy mixing and examine the variation of monolayer-averaged strain and quadrupolar quantities along the growth axis, using Gaussian envelope-square weighting. In all cases the quantities show a rather flat profile along the growth axis up until the top two monolayers. It can be observed that compared to pure InAs case, a substitution of 30% of Ga changes the overall QD strain state in such a way that both ϵ_{zz} and ϵ_B are reduced, and in corollary, so is the energy splitting, ν_Q . On the other hand the tilt angle of the major quadrupolar axis from the growth axis, $\theta_{z,Q}$ is larger caused by the local random alloy configurations. A large $\theta_{z,Q}$ has a number of implications such as enhancing the NCSHFI as will be discussed later. These observations are further supported quantitatively in Table II which compares the statistics of ϵ_{\perp} , ϵ_S , ϵ_B , ν_Q , η , $\theta_{z,\epsilon}$, and $\theta_{z,Q}$ for three different alloy compositions. With the reduction of indium composition from the pure InAs case, the in-plane and biaxial strain diminishes as well as

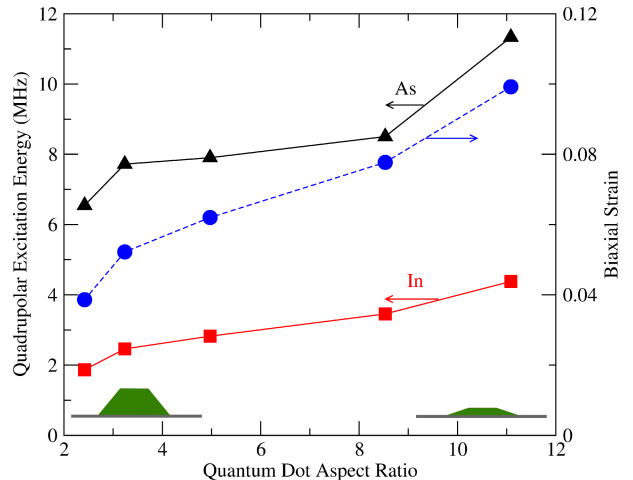


FIG. 3. (Color online) Aspect ratio (defined as the base diameter over the height) dependence of ϵ_B and ν_Q for an InAs QD. Base (top) diameter is kept at 25 nm (10 nm) while the QD height is varied. Envelope-square-weighted values are used.

the quadrupolar energy splitting, whereas, the increased random alloying enhances the EFG biaxiality and causes substantial deviation of the major strain and quadrupolar axes from the growth axis especially for the As and Ga nuclei.

Finally, we consider the role of aspect ratio of the QD on the strain and quadrupolar state. To begin with, if we were to have a *spherical* QD embedded into a host of a different lattice constant, in the continuum approximation we would have only a hydrostatic strain and no biaxial strain and no quadrupolar shift. In accordance with this, as seen in Fig. 3, QDs with a large aspect ratio possess a larger biaxial strain causing large quadrupolar shifts. Note that due to the truncated cone shape, an anisotropy always remains regardless of the height of the QD. In self-assembled QDs, while the height is controlled to a very high precision, such as by capping and double capping techniques,³⁸ this is not the case for the lateral dimension which is essentially determined by the local growth kinetics.¹⁰ Therefore, we can expect a significant

TABLE II. The effect of alloy composition on the Gaussian envelope-square-weighted statistics for the same atomistic quantities considered in Table I. Three different alloy compositions are compared for a $\text{In}_x\text{Ga}_{1-x}\text{As}$ QD: $x = 1, 0.7, \text{ and } 0.4$.

	Indium			Arsenic			Gallium	
	$x=1$	$x=0.7$	$x=0.4$	$x=1$	$x=0.7$	$x=0.4$	$x=0.7$	$x=0.4$
ϵ_{\perp}	-0.057	-0.046	-0.024	-0.056	-0.045	-0.018	-0.044	-0.015
ϵ_S	0.004	0.008	0.008	0.005	0.011	0.011	0.008	0.008
ϵ_B	0.090	0.067	0.034	0.086	0.065	0.031	0.068	0.033
ν_Q (MHz)	3.974	3.846	2.346	9.804	8.048	1.677	4.555	2.037
η	0.042	0.198	0.431	0.117	0.414	0.584	0.239	0.476
$\theta_{z,\epsilon}$	89.3°	87.7°	82.3°	88.0°	86.3°	74.5°	88.3°	70.5°
$\theta_{z,Q}$	1.7°	3.2°	12.4°	12.9°	17.9°	41.5°	5.3°	17.4°

variance on the quadrupolar shifts from dot to dot within the same sample, much like their light emission properties.

C. NMR spectra

Now, including a dc magnetic field, \mathbf{B}_0 , both Faraday and Voigt geometries will be discussed where \mathbf{B}_0 is parallel and perpendicular to the (optical) growth axis, respectively. In Fig. 4 the QZ spectra of a single In and As nuclei are given. For the quadrupolar parameters we use those listed in Table I under the envelope-squared QD statistics. Some of the comparisons regarding the quadrupolar splittings between As and In were already made in the previous section. Here, we would like to focus on the evolution of the QZ spectra from the quadrupolar-to the Zeeman-dominated regime. One can easily realize the marked discrepancy between the Faraday and Voigt geometries: in the former, as the magnetic field is increased the quadrupolar-split $m = +I$ state, moves down in energy through a number of band crossings followed by a final anticrossing. The couplings are localized to the vicinity of these ‘‘crossings’’. In the case of Voigt geometry however, there are no such band crossings. The fundamental difference is illustrated in Fig. 5. Most importantly, QI being a rank-two tensor has a *bilateral* axis because of which there remains the $\pm m$ degeneracy in its spectrum, whereas the magnetic field is vectorial, i.e., *unilateral*. In the Faraday geometry, as the field increases the system loses its bilateral character while slightly rotating to align with the magnetic axis. In the Voigt geometry, almost orthogonal setting of the two axes causes *all* the states to be mixed as the system evolves, as can be seen from the corresponding QZ spectra.

We shall now make use of the QZ spectra in interpreting the NMR absorption spectra. To excite the nuclear spins a linearly polarized rf magnetic field perpendicular to \mathbf{B}_0 is introduced. If EFG were both uniaxial (i.e., $\eta = 0$) and its major principal axis were collinear with \mathbf{B}_0 then only a perpendicular rf magnetic field would cause transitions. In our QDs where these assumptions do not hold, we observed that an rf field *parallel* to \mathbf{B}_0 also couples to nuclear spins yielding a similar spectra. However,

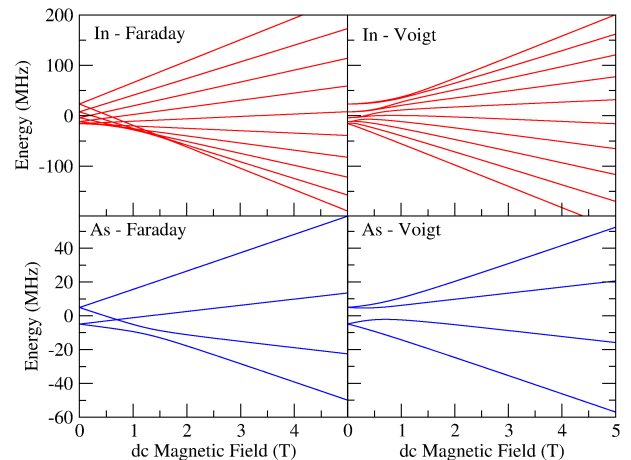


FIG. 4. (Color online) QZ spectra of single In and As nuclei for the Faraday and Voigt geometries. Z designates the major quadrupolar axis, and \mathbf{B}_0 the dc magnetic field direction.

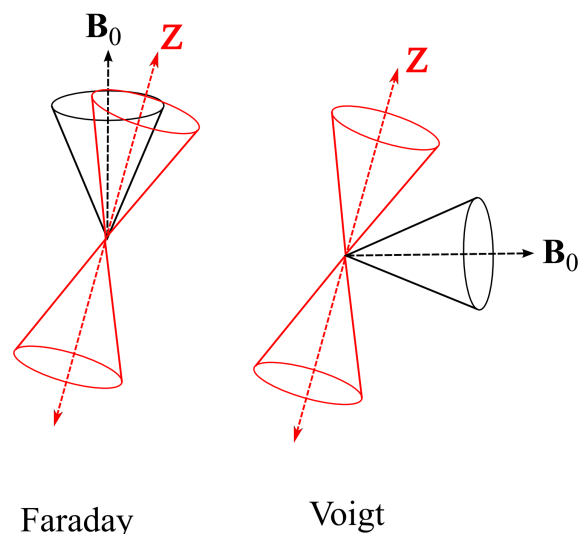


FIG. 5. (Color online) Illustration of the magnetic field and quadrupolar axes for Faraday and Voigt geometries. The single- and bi-cones represent the $|I\rangle$ and $|\pm I\rangle$ states for the Zeeman and quadrupolar cases, respectively.

their intensity is about two orders of magnitude weaker, and for this reason will not be included here. We assume that initially all nuclear spin states are equally populated giving rise to *full* spectra which can be justified based on the much smaller energy separations among QZ states with respect to thermal energy at few Kelvins, as well as due to the presence of dipole-dipole interactions among the nuclei.^{35,36} As a caveat, we would like to point out that some *parts* of the full spectra, to be discussed below, can become hindered depending on how the nuclear spin ensemble gets prepared under various experimental realizations.

The NMR spectra of InAs and $\text{In}_{0.7}\text{Ga}_{0.3}\text{As}$ QDs are shown in Figs. 6 and 7 for Faraday and Voigt geometries, respectively. To assist their interpretation we also include those of the element-resolved and single nucleus spectra as well. As a matter of fact, the fingerprints of the single nucleus spectra can be readily identified on the overall QD cases. Not observing In nuclei in the Voigt geometry NMR spectra, Flisinski *et al.* attributed this to the 2.5 times smaller population of each spin state compared to a spin-3/2 nucleus.⁶³ However, our predictions show that In nuclei must have stronger rf absorption intensity compared to As which stems from the γI^2 dependence in the rate expression (cf. Appendix); together with the aforementioned population discrepancy this results in an overall factor of about five in favor of In over As. For this reason, In nuclei are dominant on the total spectra. As marked in the Faraday geometry of single nucleus cases, a borderline between the quadrupolar and Zeeman regimes can be introduced which corresponds to about 1.1 T for the As and 1.5 T for the In nucleus. These can be taken as the effective magnetic fields, B_Q up to which QI is strong. Even though it is not as distinct, one can observe that same values also hold for the Voigt geometry. The transitions among m states are also labeled on the single As nucleus with its simpler spectrum, where we use on either side of B_Q the asymptotic pure quadrupolar or pure Zeeman basis. For each case individually, the selection rule is⁶⁶ $\Delta m = \pm 1$, however, EFG biaxiality or the noncollinear EFG axis with respect to \mathbf{B}_0 introduce higher-order transitions albeit with much weaker strength.

The severity of the inhomogeneous broadening can be clearly observed from a comparison between the single nucleus and element-resolved spectra. As expected, the higher-order transitions which are forbidden in the absence of QI are highly broadened because of the atomistic level strain variation over the QD to which they owe their existence. If we now focus on the overall spectra, we observe that for Faraday geometry, the so-called central transition, $1/2 \rightarrow -1/2$ is the sharpest among all, even in the presence of alloy mixing in $\text{In}_{0.7}\text{Ga}_{0.3}\text{As}$, with the reason being that for this transition QI has no influence.⁶⁷ On the other hand for the Voigt geometry *all* of single-nucleus resonances are broadened due to orthogonality of the quadrupolar axis with respect to \mathbf{B}_0 .

In Fig. 8 we compare the NMR spectra at 1 and 5 T

for the Faraday and Voigt geometries. Note that to gain a broader insight to the compositional effects we also include the $\text{In}_{0.4}\text{Ga}_{0.6}\text{As}$ case. Once again it can be verified that for the Faraday geometry the central line of all QDs coincide with the same sharp linewidth (marked by the vertical arrow in the 5 T case). A pivotal observation is that the $\text{In}_{0.7}\text{Ga}_{0.3}\text{As}$ and $\text{In}_{0.4}\text{Ga}_{0.6}\text{As}$ QDs have progressively narrower overall spectral support with respect to InAs case. This effect of alloying reminds the motional narrowing in the case of atomic gases,^{35,36} however, in this case caused by quite a different reason, where the spin-9/2 manifolds of the In nuclei are partially replaced by the spin-3/2 manifolds of the Ga nuclei, with the latter having much narrower span. Therefrom this simply suggests that the NMR spectra, especially in the Faraday geometry can be utilized to extract the indium mole fraction, which is one of the key unknown material parameters for a specific QD under consideration.^{37,38}

D. NCSHFI-mediated nuclear spin depolarization

Finally, we discuss within the Faraday configuration the NCSHFI-mediated nuclear spin depolarization, or for that matter the polarization process as well, as it is also governed by the same matrix element (cf. Eq. 7). Here, we first need to analytically describe the initial state of a nuclear spin which is aligned with the spin of an electron in the QD. Due to the presence of the quadrupolar and external dc magnetic fields, we define the so-called, *maximally overlapping* QZ state with that of a free nuclear spin along the electron spin direction. In the inset of Fig. 9 we see the evolution of the maximally-aligned state through a number of band “crossings” over the QZ states. The total out-transition time from such a state, hence the depolarization time, for an individual In or As nucleus under the mean quadrupolar field values (taken from Table I) are shown in Fig. 9. We observe that the depolarization is enhanced when the initial maximally-aligned state goes through band crossings with other QZ states, and the broader minimum occurs with the final band anticrossing. In the case of alloy mixing (dashed lines) larger tilt of the EFG axis from the growth direction in general causes rapid depolarization and the minimum magnetic field that this occurs also decreases. The minimum NCSHFI-mediated depolarization is seen to be on the order of an hour.⁶⁴ Just as in the NMR spectra, above B_Q level where Zeeman regime takes over, the NCSFHI gradually becomes weaker.

IV. CONCLUSIONS

The progress of the optically detected NMR techniques assure that the manipulation of a few-number-nuclei will not be a distant future.^{27–30,63} In line with this prospect, we present the strain and quadrupolar fields that these nuclei are exposed to at an atomistic level. First we

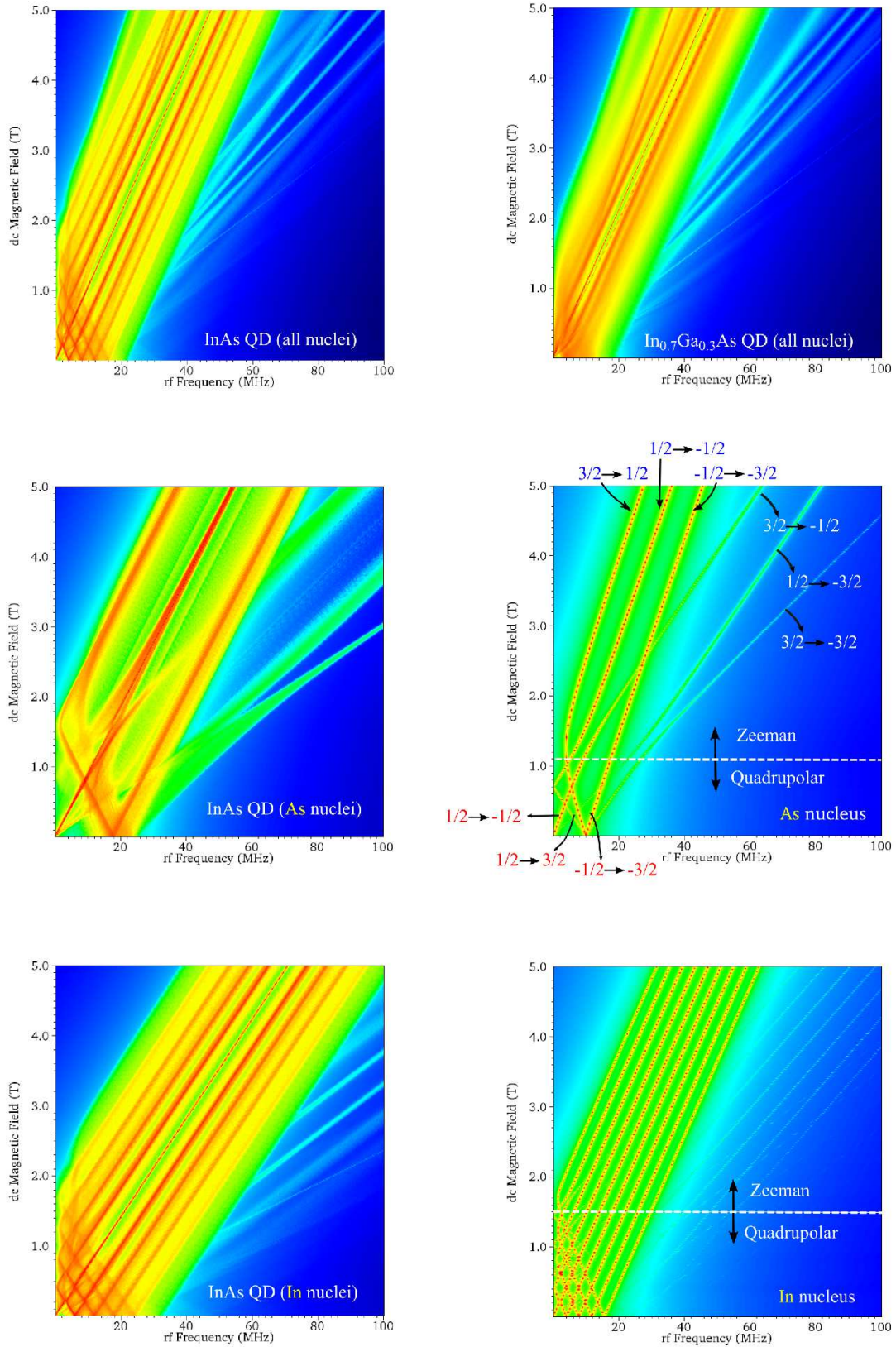


FIG. 6. (Color online) NMR spectra for InAs and In_{0.7}Ga_{0.3}As QD nuclei for the Faraday geometry (top row), together with their element-resolved As (center row) and In (bottom row) contributions for the InAs QD (left) contrasted with respective single-nucleus spectra (right).

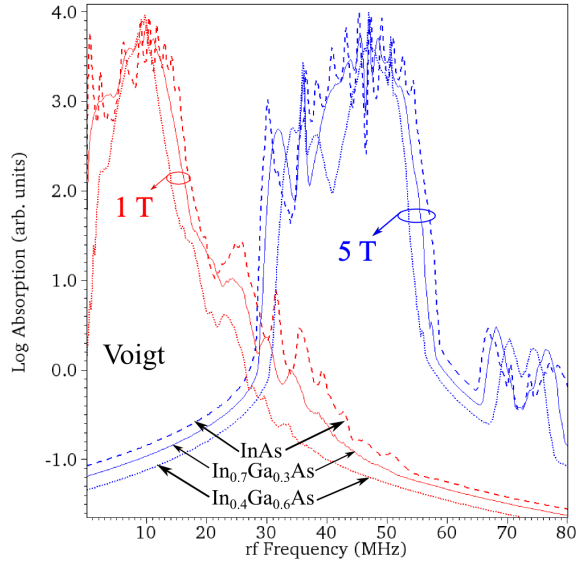
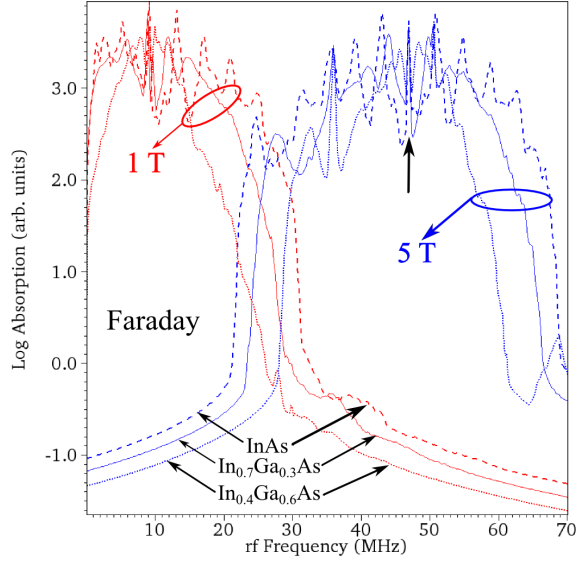


FIG. 8. (Color online) Comparison of NMR spectra at 1 and 5 T for InAs (dashed), $\text{In}_{0.7}\text{Ga}_{0.3}\text{As}$ (solid), and $\text{In}_{0.4}\text{Ga}_{0.6}\text{As}$ (dotted) QDs. Upper (lower) plot is for the Faraday (Voigt) geometry.

summarize several structural and compositional underpinnings: A high aspect ratio enhances the QI, and the interface regions introduce biaxiality and the tilting of the major quadrupolar principal axis from the growth axis. On the other hand, alloy mixing of gallium into the QD reduces both the strain and the quadrupolar energy splitting. The spectra for Faraday and Voigt geometries

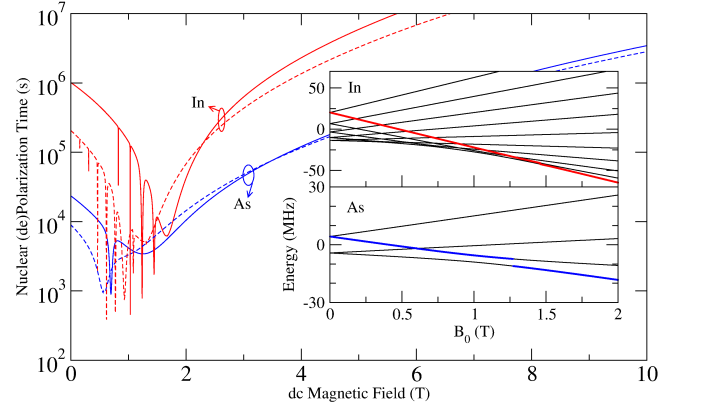


FIG. 9. (Color online) Nuclear (de)polarization time of individual In and As nuclei due to NCSHFI. QD mean EFG values are used with solid (dashed) lines for InAs ($\text{In}_{0.7}\text{Ga}_{0.3}\text{As}$). Insets show the evolution of the maximally-aligned state (high-lighted) among all QZ states as a function of magnetic field. All plots are for the Faraday geometry.

are quite distinct from each other. For the latter, all lines are inhomogeneously broadened due to the orthogonality of the quadrupolar axis with \mathbf{B}_0 . For the former, central transition, $1/2 \rightarrow -1/2$ remains sharp even in the presence of alloy mixing. Forbidden transitions are also observed, though highly broadened, arising from the EFG biaxiality and the tilting of the quadrupolar axis from the growth direction. The borderline between the quadrupolar and Zeeman regimes is extracted as 1.5 T for In and 1.1 T for As nuclei. At this value the nuclear spin depolarization rate due to the noncollinear static hyperfine interaction with a resident electron in the QD gets maximized. In the case of alloy mixing larger tilting of the EFG axis from the growth direction causes more rapid depolarization and the minimum magnetic field that this occurs also decreases. The shortest NCSHFI-mediated depolarization time is seen to be on the order of an hour. As Zeeman regime takes over above B_Q , this depolarization channel progressively becomes weaker.

ACKNOWLEDGMENTS

The author is grateful to Ataç İmamoğlu for suggesting this problem and for stimulating discussions, and thanks Martin Kroner, Javier Miguel-Sanchez, and P. M. (Paul) Koenraad for discussions regarding the experimental connection of this work, and Tahir Çağın and Dündar Yılmaz for introducing him to molecular dynamics techniques.

APPENDIX: MATRIX ELEMENTS AND RF TRANSITION RATES

In the orthogonal coordinate system as defined by the principal axes of the EFG, the dc magnetic field vector

\mathbf{B}_0 will be in general tilted as governed by the spherical polar angles θ , and ϕ so that its contribution becomes⁶⁶

$$\mathcal{H}_M = -\hbar\Omega (\mathcal{I}_X \sin \theta \cos \phi + \mathcal{I}_Y \sin \theta \sin \phi + \mathcal{I}_Z \cos \theta)$$

where $\Omega = \gamma B_0$. Choosing the angular momentum quantization axis as Z , and denoting⁵² the free nuclear spin states by $|m\rangle$, we can easily obtain the matrix elements of the parts of the full Hamiltonian as

$$\begin{aligned} \langle m' | \mathcal{H}_M | m \rangle &= -\hbar\Omega \left[m \cos \theta \delta_{m',m} + \frac{1}{2} (\sin \theta \cos \phi \right. \\ &\quad \left. \mp i \sin \theta \sin \phi) f_I(\pm m) \delta_{m',m \pm 1} \right], \\ \langle m' | \mathcal{H}_Q | m \rangle &= A_Q \left\{ [3m^2 - I(I+1)] \delta_{m',m} \right. \\ &\quad \left. + \frac{\eta}{2} f_I(\pm m) f_I(1 \pm m) \delta_{m',m \pm 2} \right\}, \end{aligned}$$

where $f_I(m) = f_I(-m-1) = \sqrt{(I-m)(I+m+1)}$, and $A_Q = \frac{e^2 q Q}{4I(2I-1)} = \frac{h\nu_Q}{6}$. Solving for the QZ spectrum essentially yields the expansion coefficients, C_m^i of the QZ states $|i\rangle$ in terms of free spin states as

$$|i\rangle = \sum_{m=-I}^I C_m^i |m\rangle. \quad (8)$$

In the case of an incident rf field, the nuclear spins are excited over their established QZ spectrum through the Hamiltonian

$$\mathcal{H}_{\text{rf}} = -\hbar\gamma \underbrace{\left[B_X^{\text{rf}} \mathcal{I}_X + B_Y^{\text{rf}} \mathcal{I}_Y + B_Z^{\text{rf}} \mathcal{I}_Z \right]}_{\mathcal{H}'}} \cos \omega_{\text{rf}} t. \quad (9)$$

Hence, based on Fermi's golden rule the rf absorption rate from an initial state $|i\rangle$ to any final state $|j\rangle$ will be

$$W_{ji}^{\text{rf}}(\omega_{\text{rf}}) = |\langle j | \mathcal{H}' | i \rangle|^2 \frac{2\Delta/\hbar}{(E_j - E_i - \hbar\omega_{\text{rf}})^2 + \Delta^2}, \quad (10)$$

where Δ is the fundamental linewidth of an individual nuclear spin for which we take 10 kHz for all the nucleus types in this work.⁶⁷ The corresponding matrix element is then given by

$$\begin{aligned} \langle j | \mathcal{H}' | i \rangle &= -\hbar\gamma \sum_{m=-I}^I B_Z^{\text{rf}} (C_m^j)^* C_m^i m \\ &\quad + B_-^{\text{rf}} (C_{m+1}^j)^* C_m^i f_I(m) \\ &\quad + B_+^{\text{rf}} (C_{m-1}^j)^* C_m^i f_I(-m) \end{aligned}$$

where $B_{\pm}^{\text{rf}} = (B_X^{\text{rf}} \pm B_Y^{\text{rf}})/2$. In the context of NCSHF1 having essentially the same matrix element $\langle j | \mathcal{I}_z | i \rangle$, one has to replace the components of \mathbf{B}^{rf} in the above expression with the components of the unit vector along the growth axis, \mathbf{z} expressed in the EFG coordinate system.

* bulutay@fen.bilkent.edu.tr

- ¹ A. V. Khaetskii, D. Loss, and L. Glazman, Phys. Rev. Lett. **88**, 186802 (2002).
- ² I. A. Merkulov, A. L. Efros, and M. Rosen, Phys. Rev. B **65**, 205309 (2002).
- ³ R. de Sousa and S. Das Sarma, Phys. Rev. B **67**, 033301 (2003).
- ⁴ B. E. Kane, Nature (London) **393**, 133 (1998).
- ⁵ J. M. Taylor, C. M. Marcus, and M. D. Lukin, Phys. Rev. Lett. **90**, 206803 (2003).
- ⁶ J. R. Petta, A. C. Johnson, J. M. Taylor, E. A. Laird, A. Yacoby, M. D. Lukin, C. M. Marcus, M. P. Hanson, and A. C. Gossard, Science **309**, 2180 (2005).
- ⁷ J. Fischer and D. Loss, Science **324** 1277 (2009).
- ⁸ H. Bluhm, S. Foletti, I. Neder, M. Rudner, D. Mahalu, V. Umansky, and A. Yacoby, Nature Phys. **7**, 109 (2011).
- ⁹ R.-B. Liu, W. Yao, and L. J. Sham, Adv. Phys. **59**, 703 (2010).
- ¹⁰ J. Stangl, V. Holý, and G. Bauer, Rev. Mod. Phys. **76**, 725 (2004).
- ¹¹ P. Petroff, Top. Appl. Phys. **90**, 1 (2003).
- ¹² C. W. Lai, P. Maletinsky, A. Badolato, and A. Imamoglu, Phys. Rev. Lett. **96**, 167403 (2006).
- ¹³ B. Eble, O. Krebs, A. Lemaître, K. Kowalik, A. Kudelski, P. Voisin, B. Urbaszek, X. Marie, and T. Amand, Phys.

- Rev. B **74**, 081306(R) (2006).
- ¹⁴ A. I. Tartakovskii, T. Wright, A. Russell, V. I. Falko, A. B. Vankov, J. Skiba-Szymanska, I. Drouzas, R. S. Kolodka, M. S. Skolnick, P. W. Fry, A. Tahraoui, H.-Y. Liu, and M. Hopkinson, Phys. Rev. Lett. **98**, 026806 (2007).
- ¹⁵ B. Urbaszek, P.-F. Braun, T. Amand, O. Krebs, T. Belhadj, A. Lemaître, P. Voisin, and X. Marie, Phys. Rev. B **76**, 201301 (2007).
- ¹⁶ M. N. Makhonin, A. I. Tartakovskii, A. B. Vankov, I. Drouzas, T. Wright, J. Skiba-Szymanska, A. Russell, V. I. Falko, M. S. Skolnick, H.-Y. Liu, and M. Hopkinson, Phys. Rev. B **77**, 125307 (2008).
- ¹⁷ M. Kroner, K. M. Weiss, B. Biedermann, S. Seidl, S. Manus, A. W. Holleitner, A. Badolato, P. M. Petroff, B. D. Gerardot, R. J. Warburton, and K. Karrai, Phys. Rev. Lett. **100**, 156803 (2008).
- ¹⁸ X. Xu, W. Yao, B. Sun, D. G. Steel, A. S. Bracker, D. Gammon, and L. J. Sham, Nature (London) **459**, 1105 (2009).
- ¹⁹ C. Latta, A. Högele, Y. Zhao, A. N. Vamivakas, P. Maletinsky, M. Kroner, J. Dreiser, I. Carusotto, A. Badolato, D. Schuh, W. Wegscheider, M. Atature, and A. Imamoglu, Nature Phys. **5**, 758 (2009).
- ²⁰ R. V. Cherbunin, S. Yu. Verbin, T. Auer, D. R. Yakovlev, D. Reuter, A. D. Wieck, I. Ya. Gerlovin, I. V. Ignatiev,

- D. V. Vishnevsky, and M. Bayer, Phys. Rev. B **80**, 035326 (2009).
- ²¹ M. N. Makhonin, J. Skiba-Szymanska, M. S. Skolnick, H.-Y. Liu, M. Hopkinson, and A. I. Tartakovskii, Phys. Rev. B **79**, 125318 (2009).
- ²² B. Eble, C. Testelin, P. Desfonds, F. Bernardot, A. Balocchi, T. Amand, A. Miard, A. Lemaître, X. Marie, and M. Chamarro, Phys. Rev. Lett. **102**, 146601 (2009).
- ²³ O. Krebs, P. Maletinsky, T. Amand, B. Urbaszek, A. Lemaître, P. Voisin, X. Marie, and A. Imamoglu, Phys. Rev. Lett. **104**, 056603 (2010).
- ²⁴ R. V. Cherbunin, K. Flisinski, I. Ya. Gerlovin, I. V. Ignatiev, M. S. Kuznetsova, M. Yu. Petrov, D. R. Yakovlev, D. Reuter, A. D. Wieck, and M. Bayer, Phys. Rev. B **84**, 041304 (2011).
- ²⁵ F. Meier and B. P. Zakharchenya, *Optical Orientation*, (North-Holland, Amsterdam, 1984).
- ²⁶ G. Lampel, Phys. Rev. Lett. **20**, 491 (1968).
- ²⁷ D. Gammon, S. W. Brown, E. S. Snow, T. A. Kennedy, D. S. Katzer, and D. Park, Science **277**, 85 (1997).
- ²⁸ D. Gammon, A. L. Efros, T. A. Kennedy, M. Rosen, D. S. Katzer, D. Park, S. W. Brown, V. L. Korenev, and I. A. Merkulov, Phys. Rev. Lett. **86**, 5176 (2001).
- ²⁹ M. N. Makhonin, E. A. Chekhovich, P. Senellart, A. Lemaître, M. S. Skolnick, and A. I. Tartakovskii, Phys. Rev. B **82**, 161309 (2010).
- ³⁰ M. N. Makhonin, K. V. Kavokin, P. Senellart, A. Lemaître, A. J. Ramsey, M. S. Skolnick, and A. I. Tartakovskii, arXiv:1102.3636 (unpublished).
- ³¹ R. I. Dzhiyev and V. L. Korenev, Phys. Rev. Lett. **99**, 037401 (2007).
- ³² R. K. Sundfors, Phys. Rev. **177**, 1221 (1969).
- ³³ R. K. Sundfors, Phys. Rev. **185**, 458 (1969).
- ³⁴ R. K. Sundfors, Phys. Rev. B **10**, 4244 (1974).
- ³⁵ A. Abragam, *Principles of Nuclear Magnetism*, (Oxford University Press, New York, 1961).
- ³⁶ C. P. Slichter, *Principles of Magnetic Resonance*, (Springer-Verlag, Berlin, 1978) 2nd Ed.
- ³⁷ G. Biasiol and S. Heun, Phys. Rep. **500**, 117 (2011).
- ³⁸ J. M. Ulloa, P. Offermans and P. M. Koenraad, in M. Henini (Ed.), *Handbook of Self-Assembled Semiconductor Nanostructures for Novel Devices in Photonics and Electronics* (Elsevier, Amsterdam, 2008) Ch. 5, pp. 165-200.
- ³⁹ S. Plimpton, J. Comp. Phys. **117**, 1 (1995); <http://lammmps.sandia.gov>.
- ⁴⁰ G. C. Abell, Phys. Rev. B **31**, 6184 (1985); J. Tersoff, Phys. Rev. B **37**, 6991 (1988).
- ⁴¹ D. Powell, M. A. Migliorato, and A. G. Cullis, Phys. Rev. B **75**, 115202 (2007).
- ⁴² J. J. Ramsey, E. Pan, and P. W. Chung, J. Phys.: Condens. Matter **20** 485215 (2008).
- ⁴³ C. Pryor, J. Kim, L. W. Wang, A. J. Williamson, and A. Zunger, J. Appl. Phys. **83**, 2548 (1998).
- ⁴⁴ G. Bester, X. Wu, D. Vanderbilt, and A. Zunger, Phys. Rev. Lett. **96**, 187602 (2006).
- ⁴⁵ In this paper lower case x , y , and z refer to cubic crystallographic axes with z being the growth direction, whereas upper case X , Y , and Z are used for EFG principal axes such that $|V_{XX}| \leq |V_{YY}| \leq |V_{ZZ}|$, i.e., the major principal axis chosen along Z . Needless to say, shear and biaxial components are specified in crystallographic and EFG frames, respectively.
- ⁴⁶ R. G. Shulman, B. J. Wyluda, and P. W. Anderson, Phys. Rev. **107**, 953 (1957).
- ⁴⁷ Our notation slightly deviates from Ref. 46. Throughout this work we make use of tensor strains as opposed to engineering strains.⁴⁸
- ⁴⁸ J. F. Nye, *Physical Properties of Crystals* (Oxford University Press, 1985).
- ⁴⁹ R. J. Harrison and P. L. Sagalyn, Phys. Rev. **128**, 1630 (1962).
- ⁵⁰ We would like to warn about the recent proliferating use^{31,51,55,63} of the expression $V_{zz} = S_{11}\epsilon_{zz}$ which is not valid, as the major strain component that remains in a QD is ϵ_{\perp} , whereas ϵ_{zz} mostly relaxes.
- ⁵¹ E. A. Chekhovich, M. N. Makhonin, J. Skiba-Szymanska, A. B. Krysa, V. D. Kulakovskii, M. S. Skolnick, and A. I. Tartakovskii, Phys. Rev. B **81**, 245308 (2010).
- ⁵² Free nuclear spin states along a general quantization axis will be denoted by $|m\rangle$ or $|m'\rangle$, whereas those under both quadrupolar and Zeeman fields (i.e., QZ states) will be denoted by $|i\rangle$ or $|j\rangle$.
- ⁵³ C. Deng and X. Hu, Phys. Rev. B **71**, 033307 (2005).
- ⁵⁴ W. A. Coish and J. Baugh, Phys. Status Solidi B **246**, 2203 (2009).
- ⁵⁵ C. W. Huang and X. Hu, Phys. Rev. B **81**, 205304 (2010).
- ⁵⁶ P. Maletinsky, A. Badolato, and A. Imamoglu, Phys. Rev. Lett. **99**, 056804 (2007).
- ⁵⁷ P. Borri, W. Langbein, S. Schneider, U. Woggon, R. L. Sellin, D. Ouyang, and D. Bimberg, Phys. Rev. Lett. **87**, 157401 (2001).
- ⁵⁸ We also investigated lens and truncated pyramidal shaped QDs and observed no qualitative differences. To keep the discussion concise, these results are excluded.
- ⁵⁹ M. Parrinello and A. Rahman, J. Appl. Phys. **52**, 7182 (1981).
- ⁶⁰ J. Li, Modell. Simul. Mater. Sci. Eng. **11**, 173 (2003). The atomistic images are generated using the package of ATOMEYE.
- ⁶¹ M. A. Migliorato, A. G. Cullis, M. Fearn, and J. H. Jefferson, Phys. Rev. B **65**, 115316 (2002).
- ⁶² A. Schliwa, M. Winkelkemper, and D. Bimberg, Phys. Rev. B **76**, 205324 (2007).
- ⁶³ K. Flisinski, I. Ya. Gerlovin, I. V. Ignatiev, M. Yu. Petrov, S. Yu. Verbin, D. R. Yakovlev, D. Reuter, A. D. Wieck, and M. Bayer, Phys. Rev. B **82**, 081308 (2010).
- ⁶⁴ However, this should not be solely attributed NCSHFI, as it requires the presence of co-tunneling and hence a resident electron in the dot, without which there is no nuclear spin decay at any finite field.⁶⁵
- ⁶⁵ C. Latta, A. Srivastava, and A. Imamoglu, Phys. Rev. Lett. **107**, 167401 (2011).
- ⁶⁶ T. P. Das and E. L. Hahn, *Nuclear Quadrupole Resonance Spectroscopy* (Academic Press Inc., New York, 1958).
- ⁶⁷ D. Mao and P. C. Taylor, Phys. Rev. B **52**, 5665 (1995).